REEF3D::FNPF - A Flexible Fully Nonlinear Potential Flow Solver

Hans Bihs, Weizhi Wang*, Csaba Pakozdi, Arun Kamath
Department of Civil and Environmental Engineering, Norwegian University of Science and Technology (NTNU), 7491 Trondheim, Norway

J. Offshore Mech. Arct. Eng., 2020, **1142** 4, pp. .
DOI: http://dx.doi.org/https://doi.org/10.1115/1.4045915

Abstract

In situations where the calculation of ocean wave propagation and impact on offshore structures is required, fast numerical solvers are desired in order to find relevant wave events. Computational Fluid Dynamics (CFD) based Numerical Wave Tanks (NWT) emphasize on the hydrodynamic details of the relevant events, such as complex wave structure interaction and breaking wave kinematics. This makes them less ideal for the event identification due to the large computational resources involved. Therefore, a computationally efficient numerical wave model is needed to identify the events both for offshore wave fields with deep water condition and coastal wave fields where the bathymetry and coastline variation have strong impact on wave propagation. In the current paper a new numerical wave model is represented that solves the Laplace equation for the flow potential and the nonlinear kinematic and dynamics free surface boundary conditions. This approach requires reduced computational resources compared to CFD based NWTs. The resulting fully nonlinear potential flow solver REEF3D::FNPF uses a σ-coordinate grid for the computations. This allows the grid to follow the irregular bottom variation with great flexibility. The free surface boundary conditions are discretized using fifth-order WENO finite difference methods and the third-order TVD Runge-Kutta scheme for time stepping. The Laplace equation for the potential is solved with Hypres stabilized bi-conjugated gradient solver preconditioned with geometric multi-grid. REEF3D::FNPF is fully parallelized following the domain decomposition strategy and the MPI communication protocol. The model is successfully tested for wave propagation benchmark cases for shallow water conditions with variable bottom as well as deep water. The numerical results agree well with the experimental measurements in all tested cases and the model proves to be efficient and accurate for both offshore and coastal conditions.

Keywords: Fully non-linear potential flow; Numerical wave modelling; Irregular topography; REEF3D

*Corresponding author, weizhi.wang@ntnu.no
Postprint, published in J. Offshore Mech. Arct. Eng., doi: http://dx.doi.org/https://doi.org/10.1115/1.4045915

1 Introduction

In the study of wave propagation and wave loads on offshore and coastal structures, phase-resolved wave modeling is often required, because it presents the details of the complicated free surface phenomena and enables a time domain analysis. A closer investigation of wave-structure interaction usually requires a Navier-Stokes solver to represent the complicated events involving turbulent flows. REEF3D is developed as an open-source hydrodynamic model specializing in the simulations of complex free surface flows Bihs et al. (2016). Its Navier-Stokes solver REEF3D::CFD has been widely used for various hydrodynamic studies. For example, the model is used for the regular wave interaction with surface piercing circular cylinder arrays Kamath et al. (2016), wave interaction with horizontal semi-submersible cylinders in tandem Ong et al. (2017) and multi-directional irregular wave interaction with a large-diameter cylinder Wang et al. (2018). The modular design of the model enables a flexible implementation of extensions. As a result, the model is also seen in a broader range of applications, such as the sediment transport analysis Ahmad et al. (2018) and the coastal infrastructure design Sasikumar et al. (2018). However, such computations tend to require a high resolution of the computational domain and therefore require more computational resources and longer simulation time. In order to identify relevant wave events close to the structures, a large-scale simulation is demanded, where a faster numerical model is needed.

In the far-field wave domain, fast two-dimensional shallow water models have been developed for fast phase-resolving wave modeling, such as widely used Boussinesq-type models Madsen et al. (1991); Nwogu (1993). However, the representation of the dispersion relation remains a challenge in deep water regions with such models. Turbulence and viscosity are normally not significant in the far-field domain. Therefore, a potential flow solver is ideal for a fast calculation of wave propagation in the far-field, especially in deep water conditions. The development of the potential flow solvers has focused on the representation of nonlinearity. One nonlinear wave model in the potential flow domain is the high-order spectrum (HOS) model Ducrozet et al. (2012); Ducrozet et al. (2016) where a high level of accuracy and computational efficiency are provided by a Fast Fourier Transform (FFT) solution. The model is proven to be efficient both in a numerical wave tank and in an open-ocean scenario. However, the development is challenged by an efficient representation of the fast varying bottom geometry.

Another approach is solving the Laplace equation with an enclosure of free surface boundary conditions and the bottom boundary condition. In the studies of Grilli et al. (1996) Grilli (1996), a high-order boundary element method (BEM) is used for various applications including wave propagation, shoaling, breaking and wave run-up. Correct representations of both the geometry and kinematics of strongly nonlinear waves are achieved with the highly nonlinear model where no approximations are introduced for the free surface boundary conditions. However, BEM approaches usually require explicit knowledge of a fundamental solution of the differential equations and case-specific mathematical analysis. A sharp discontinuity at the boundary, such as corners and edges may introduce singularities in the solution. In contrast to the BEM approach, Li and Fleming (1997) Li and Fleming (1997) were the first to propose a finite difference method (FDM) for the solution of the Laplace equation throughout the whole domain. A low-order multi-grid method is developed for an efficient and scalable solution of the fully nonlinear potential flow (FNPF) equations for water wave applications. Bingham et al. (2007) Bingham and Zhang (2007) further improved the model using high-order finite

differences. In 2008, OceanWave3D Engsig-Karup et al. (2009) was introduced as a fully nonlinear and dispersive free surface wave model for 3D nonlinear water waves. Adaptive and curvilinear meshes are employed in the model, offering flexibilities with respect to geometry. The model has also been extended to study wave-structure interactions Engsig-Karup and Bingham (2009); Ducrozet et al. (2014). However, the mesh generation with curvilinear mesh can be challenging with the appearance of complicated solid boundaries in the computational domain. Other FNPF models have also been developed in 2D or 3D, as presented in Janssen et al. (2010); Mehmood et al. (2015, 2016). These FNPF models are able to simulate strongly nonlinear wave generation, propagation and transformation, up to wave overturning Janssen et al. (2010). Recently, much attention has also been put on improving the computational capacity of the FNPF models. For example, an OceanWave3D version equipped with a GPU-based parallelization was introduced in 2012 Engsig-Karup et al. (2012). Further explanations of the GPU implementations on heterogeneous many-core architectures can be found in Engsig-Karup et al. (2013) and Glimberg et al. (2013). The model achieves an applaudable computational efficiency, but also requires specific GPU infrastructure.

There is a lack of potential flow model that represents both non-linear wave phenomena at offshore and wave transformation at coastal area with irregular varying topography, as well as supporting High Performance Computation (HPC) with multiple processors. In this paper, a fully nonlinear potential flow solver REEF3D::FNPF is introduced in the numerical framework of REEF3D. The computations are performed with a finite difference method on a σ-coordinate grid. Since the model is coded in REEF3D, the existing robust numerical schemes in REEF3D are straightforward accessible to the proposed model. For example, the model is equipped with high-order discretization schemes and is fully parallelized with an MPI-based domain decomposition method. The presented paper describes the governing equations and the numerical implementations of the model. Then four test cases are shown to demonstrate its numerical performance. First, a linear progressive wave propagation over constant water depth is simulated. Then, the wave propagation over irregular topography is investigated by simulating the wave transformation over a submerged bar. Next, the evolution of a wave packet and the wave focusing is presented. Finally, a three-hour irregular wave simulation is performed. The simulated results are compared to theoretical values and experimental measurements. In the presented studies, the model shows a robust accuracy and cheerful computational efficiency.

2 Numerical Model

Governing equations

The governing equation for the flow calculations in the open-source fully non-linear potential flow code REEF3D::FNPF is the Laplace equation:

$$\frac{\partial^2 \phi}{\partial x^2} + \frac{\partial^2 \phi}{\partial y^2} + \frac{\partial^2 \phi}{\partial z^2} = 0 \tag{1}$$

In order to solve for the velocity potential ϕ, this elliptic equation requires boundary conditions, where especially the ones at the free surface and the bed are of importance. At the free surface, the fluid particles should remain at the surface and the pressure in the fluid

is equal to the atmospheric pressure. These conditions must hold true at the free surface at all times and they form the kinematic and dynamic boundary conditions at the free surface respectively:

$$\frac{\partial \eta}{\partial t} = -\frac{\partial \eta}{\partial x}\frac{\partial \widetilde{\phi}}{\partial x} - \frac{\partial \eta}{\partial y}\frac{\partial \widetilde{\phi}}{\partial y} + \widetilde{w}\left(1 + \left(\frac{\partial \eta}{\partial x}\right)^2 + \left(\frac{\partial \eta}{\partial y}\right)^2\right), \tag{2}$$

$$\frac{\partial \widetilde{\phi}}{\partial t} = -\frac{1}{2}\left(\left(\frac{\partial \widetilde{\phi}}{\partial x}\right)^2 + \left(\frac{\partial \widetilde{\phi}}{\partial y}\right)^2\right) + \frac{1}{2}\widetilde{w}^2\left(1 + \left(\frac{\partial \eta}{\partial x}\right)^2 + \left(\frac{\partial \eta}{\partial y}\right)^2\right) - g\eta. \tag{3}$$

where $\widetilde{\phi} = \phi(\mathbf{x}, \eta, t)$ is the velocity potential at the free surface, $\mathbf{x} = (x, y)$ represents the horizontal location and $\widetilde{w}$ is the vertical velocity at the free surface.

At the bottom, the fluid particle cannot penetrate the solid boundary, and therefore the vertical water velocity must be zero at all times. This gives the bottom boundary condition:

$$\frac{\partial \phi}{\partial z} + \frac{\partial h}{\partial x}\frac{\partial \phi}{\partial x} + \frac{\partial h}{\partial y}\frac{\partial \phi}{\partial y} = 0, \quad z = -h. \tag{4}$$

where $h = h(\mathbf{x})$ is the water depth from the seabed to the still water level.

The Laplace equation, together with the enclosure of the boundary conditions are solved on a flexible-order finite difference scheme on a σ-coordinate. The σ-coordinate can be transferred from a Cartesian grid following:

$$\sigma = \frac{z + h\left(\mathbf{x}\right)}{\eta(\mathbf{x}, t) + h(\mathbf{x})} \tag{5}$$

The velocity potential is denoted as Φ after the σ-coordinate transformation. Then the governing equations and boundary conditions in the σ-coordinate become:

$$\Phi = \widetilde{\phi}, \qquad \sigma = 1; \tag{6}$$

$$\frac{\partial^2 \Phi}{\partial x^2} + \frac{\partial^2 \Phi}{\partial y^2} + \left(\frac{\partial^2 \sigma}{\partial x^2} + \frac{\partial^2 \sigma}{\partial y^2}\right)\frac{\partial \Phi}{\partial \sigma} + 2\left(\frac{\partial \sigma}{\partial x}\frac{\partial}{\partial x}\left(\frac{\partial \Phi}{\partial \sigma}\right) + \frac{\partial \sigma}{\partial y}\frac{\partial}{\partial y}\left(\frac{\partial \Phi}{\partial \sigma}\right)\right) + \left(\left(\frac{\partial \sigma}{\partial x}\right)^2 + \left(\frac{\partial \sigma}{\partial y}\right)^2 + \left(\frac{\partial \sigma}{\partial z}\right)^2\right)\frac{\partial^2 \Phi}{\partial \sigma^2} = 0, \qquad 0 \leq \sigma < 1; \tag{7}$$

$$\left(\frac{\partial \sigma}{\partial z} + \frac{\partial h}{\partial x}\frac{\partial \sigma}{\partial x} + \frac{\partial h}{\partial y}\frac{\partial \sigma}{\partial y}\right)\frac{\partial \Phi}{\partial \sigma} + \frac{\partial h}{\partial x}\frac{\partial \Phi}{\partial x} + \frac{\partial h}{\partial y}\frac{\partial \Phi}{\partial y} = 0, \qquad \sigma = 0. \tag{8}$$

Once the velocity potential Φ is obtained in the σ-domain, the velocities can be calculated as follows:

$$u\left(\mathbf{x},z\right)=\frac{\partial\Phi\left(\mathbf{x},z\right)}{\partial x}=\frac{\partial\Phi\left(\mathbf{x},\sigma\right)}{\partial x}+\frac{\partial\sigma}{\partial x}\frac{\partial\Phi\left(\mathbf{x},\sigma\right)}{\partial\sigma}, \tag{9}$$

$$v\left(\mathbf{x},z\right)=\frac{\partial\Phi\left(\mathbf{x},z\right)}{\partial y}=\frac{\partial\Phi\left(\mathbf{x},\sigma\right)}{\partial y}+\frac{\partial\sigma}{\partial y}\frac{\partial\Phi\left(\mathbf{x},\sigma\right)}{\partial\sigma}, \tag{10}$$

$$w\left(\mathbf{x},z\right)=\frac{\partial\Phi\left(\mathbf{x},z\right)}{\partial z}=\frac{\partial\sigma}{\partial z}\frac{\partial\Phi\left(\mathbf{x},\sigma\right)}{\partial\sigma}. \tag{11}$$

The waves are generated at the wave generation zone using the relaxation method Mayer et al. (1998). The relaxation function proposed by Jacobsen Jacobsen et al. (2012) is used in the model, as shown in Eqn. (12). In the wave generation zone, the free-surface elevation and velocities are ramped up to the designed theoretical values. In the numerical beach, a reverse process takes place and the flow properties are restored to hydrostatic values following the relaxation method.

$$\Gamma(\widetilde{x})=1-\frac{e^{(\widetilde{x}^{3.5})}-1}{e-1}\ for\ \widetilde{x}\in[0;1] \tag{12}$$

where $\widetilde{x}$ is scaled to the length of the relaxation zone.

The Laplace equation is solved using the parallelized geometric multi-grid algorithm provided by hypre van der Vorst (1992). Second-order central differences are used for the discretization of the Laplace equation.

The calculation of wave propagation can be challenging because insufficient grid resolution can cause numerical diffusion which consequently leads to unphysical damping of the waves. In order to achieve the balance between the order of accuracy of the discretization methods and the numerical stability and efficiency, the model chooses the fifth-order WENO (weighted essentially non-oscillatory) scheme Jiang and Shu (1996) in the conservative finite-difference framework for the discretization of the convection terms. This scheme can handle large gradients accurately by taking local smoothness into account. The overall WENO discretization stencil consists of three local ENO-stencils, which are weighted depending on their smoothness, with the smoothest stencil contributing the most significantly.

For the time treatment for the freesurface boundary conditions, a third-order accurate TVD Runge-Kutta scheme Shu and Osher (1988) is used. Adaptive time stepping is used in order to determine the time step size while keeping a constant CFL number which is based on phase velocity.

The model is fully parallelized following the domain decomposition strategy. Ghost cells are used within the implemented domain decomposition framework for the parallelization. These ghost cells are updated with the values from the neighboring processors via MPI (Message Passing Interface).

3 Results

Linear wave propagation

At first, the proposed model is tested with wave propagation over a constant bottom. The two-dimensional (2D) numerical wave tank is 35 m long. The still water level is constant at

0.4 m. The input wave is a linear wave at intermediate water depth. The wave height is 0.02 m and the wavelength is 3.73 m. A wave generation zone of one wavelength is located at the inlet of the tank to the left-hand side. A numerical beach of two wavelengths is located at the outlet of the tank to the right-hand side. The schematics of the numerical wave tank's configuration is shown in Fig. 1.

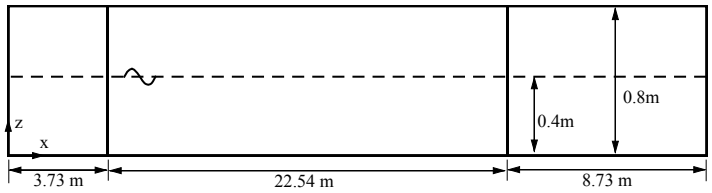

Figure 1: The configuration of the numerical wave tank for the linear wave propagation.

To study the grid convergence property of the model, three simulations are performed with three different grid sizes. The finest grid uses 85 cells per wavelength, the intermediate grid allows 53 cells per wavelength, while the coarsest grid consists of 26 cells per wavelength. The wave profiles at $t = 35$ s from the three simulations are compared to the theoretical value in Fig. 2:

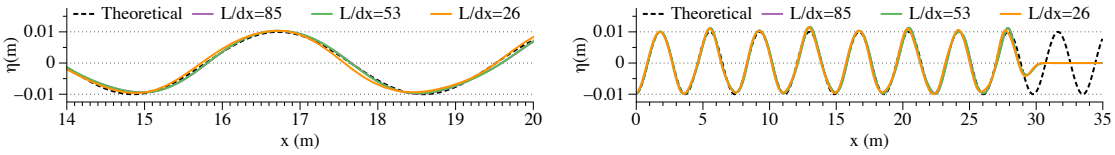

(a) (b)

Figure 2: The comparison of the wave profile at $t = 35$ s for the linear wave propagation. (a) the comparison along the whole tank, (b) a closer view at the wave profile.

A Richardson extrapolation method is used to estimate the grid-independent numerical result, the spatial discretization error and the convergence rate. The average wave heights during 30 s simulations are used for the grid-convergence study. The fitted curve of the Richardson extrapolation is shown in Fig. 3. It is seen that the grid-independent average wave height is 0.01983 m, with an error of -0.833% compared to the input theoretical value of 0.01983 m. The monotonic convergence rate is found to be 2.64, higher than second order.

Wave propagation over a submerged bar

In this section, the wave propagation over a submerged bar Beji and Battjes (1993) is tested. The 2D wave tank of 35 m is equipped with a wave generation zone of one wavelength 3.73 m at the inlet and a numerical beach of two wavelengths 8.73 m at the outlet. The still water level is 0.4 m. The submerged bar begins at $x = 6$ m and elevates following a slope of $1 : 20$ until it reaches the top platform at $x = 12$ m, with a height of 0.3 m. It remains the height for 2 m before it starts a downwards slope of $1 : 10$ and reaches the bottom of the tank at $x = 17$ m. Nine wave gauges are located at $x = 4.0$ m, 10.5 m, 12.5 m, 13.5 m, 14.5 m, 15.7 m, 17.3 m, 19.0 m and 21.0 m. The incident wave height is $H = 0.02$ m and the wavelength is $L = 3.73$ m. The

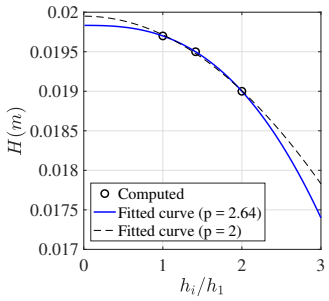

Figure 3: The grid convergence study following a Richardson extrapolation method for the linear wave propagation case.

schematics of the configurations of the numerical wave tank is shown in Fig. 4.

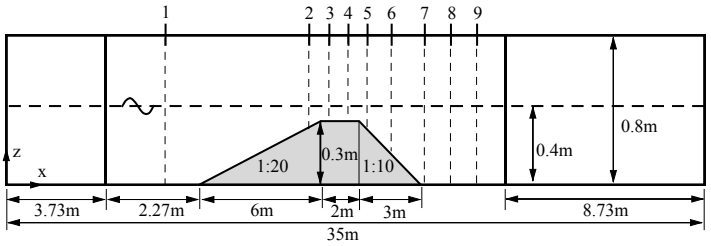

Figure 4: The configuration of the numerical wave tank for wave propagation over a submerged bar.

A grid convergence study is performed at gauge 2 and 6, before and after the crest of the submerged bar, as shown in Fig. 5a and Fig. 5b. Three grids sizes are used in the study, giving 212, 106, 53, and 26 cells per incident wavelength. It is found that 212 cells per wavelength are sufficient to capture the wave transformation. A simulation time of 35 s is used. With 12 2.7 GHz cores on a Mac Pro with 32 GB memory, the simulation only takes 170 s. The time series at all nine wave gauges are compared to the experimental measurements, shown from Fig. 6a to Fig. 6i. The waves shoal over the uprising slope of the submerged bar. A continuous increase of wave height is observed from gauge 1 to gauge 3. Gauge 4 and gauge 5 sees the beginning of the wave decomposition process, where higher frequency short wave components start to emerge. From gauge 6, the de-shoaling takes place, and the wave decomposition becomes more prominent. The velocity potential and the horizontal velocities in the numerical wave tank at $t = 35$ s is also shown in Fig. 7. With the chosen grid resolution, the evolution of the waves is well represented during the entire shoaling and the de-shoaling process, especially the complicated wave decomposition after the top of the bar. It is also noted that in order to resolve those short waves during the decomposition, a finer grid is needed compared to the previous study with a constant bottom in the previous section.

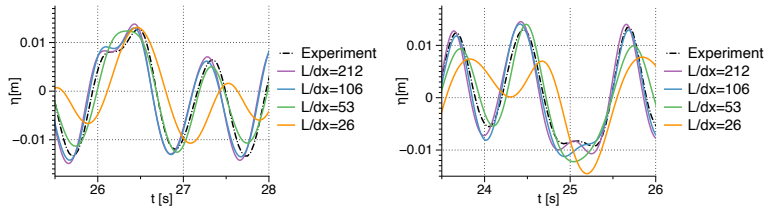

(a) Grid convergence at wave gauge 6

(b) Grid convergence at wave gauge 8

Figure 5: The grid convergence study at wave gauge 6 and wave gauge 8.

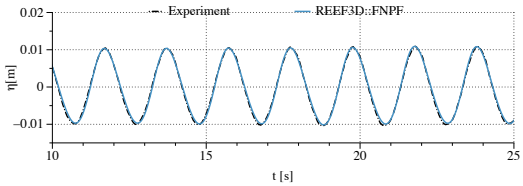

(a) wave gauge 1 at $x = 4.0$ m

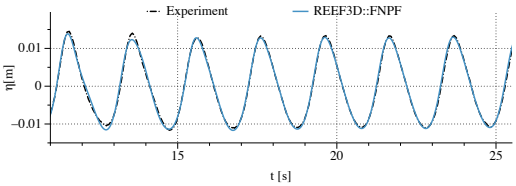

(b) wave gauge 2 at $x = 10.5$ m

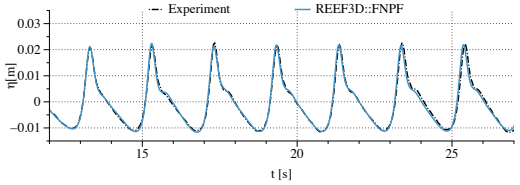

(c) wave gauge 3 at $x = 12.5$ m

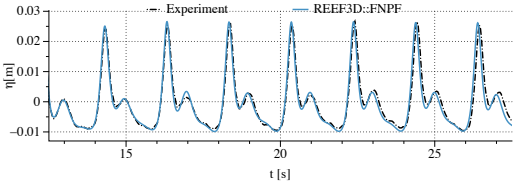

(d) wave gauge 4 at $x = 13.5$ m

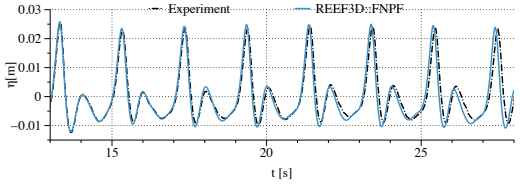

(e) wave gauge 5 at $x = 14.5$ m

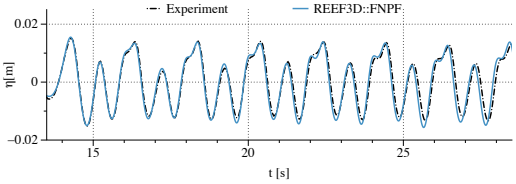

(f) wave gauge 6 at $x = 15.7$ m

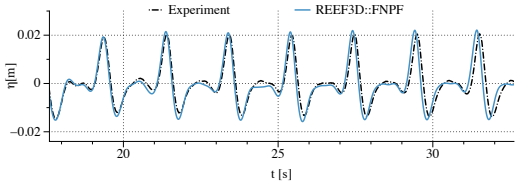

(g) wave gauge 7 at $x = 17.3$ m

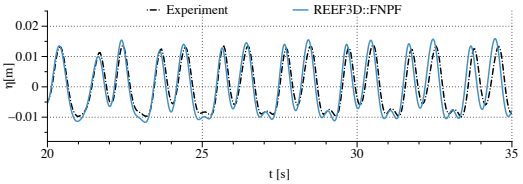

(h) wave gauge 8 at $x = 19.0$ m

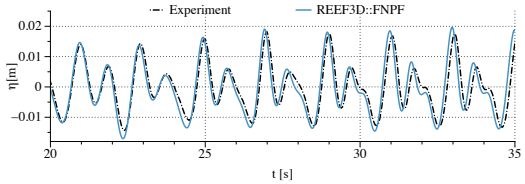

(i) wave gauge 9 at $x = 21.0$ m

Figure 6: The comparison between the simulated time series and the experimental measurements at all wave gauges with the grid resolution $L/dx = 212$ in the numerical wave tank for the wave propagation over a submerged bar.

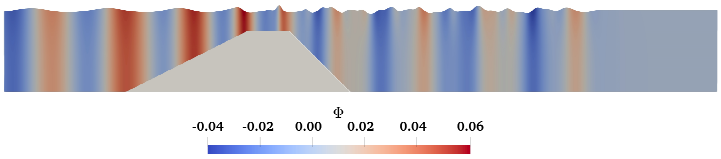

(a) The velocity potential in the wave tank at $t = 35$ s

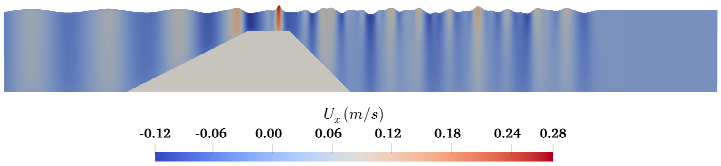

(b) The horizontal velocity in the wave tank at $t = 35$ s

Figure 7: The velocity potential and the horizontal velocity in the numerical wave tank when the waves pass the submerged bar at $t = 35$ s.

In comparison, a CFD simulation requires a much finer grid and smaller time step to resolve the high-frequency wave components. In stead of 20000 cells used in the current simulation, a cell number of 1322000 is needed in a CFD simulation to achieve good representation of the wave propagation. With 12 cores on a Mac Pro, the CFD simulation takes about 17 hours indtead of 170 s as with FNPF, a magnitude of 400 slower than the FNPF simulation for this case.

The focused wave from a wave packet

The model is tested with extreme wave event in this section. An experimental wave packet measured in the LargeWave Flume (GWK), Hannover, Germany Clauss and Steinhagen (1999) is used for the validation. Several tests in the experiment have been successfully reproduced with the CFD model REEF3D::CFD Bihs et al. (2019), including focused wave breaking. Here, a non-breaking focused wave is to be reproduced with the presented model REEF3D::FNPF. The physical wave tank in the experiment is a 300 m long channel with a still water level of $d = 4.01$ m. A Piston-type wavemaker is used to generate the wave packets such that the waves focus at a designed location and time. In the numerical test, a 2D numerical wave tank 250 m long with a water depth of $d = 4.01$ m is used. Following the arrangement from the experiment, the distance of the focus point and the time of focusing are $x_f = 126.21$ m and $t_f = 83$ s. The free surface elevations are measured at $x = 3.59$ m, 50.5 m, 79.05 m, 100.10 m and 126.21 m in the numerical wave tank. They are compared to the experimental observations as presented from Fig. 8a to Fig. 8e. The grid convergence study is shown in Fig. 9, where 30, 20 and 10 cells per shortest wavelength in the generated ave group are tested. It is found that 30 cells per shortest wavelength shows a nearly grid-independent result. With the chosen resolution, a 110 s simulation takes 1160 s with 2 processors on the same machine as shown in the previous section. At the focus location, the numerical error at the wave peak is 4.8%. In order to show the evolution of the wave packet, the wave profiles and the horizontal velocities in the computational domain are shown in Fig. 10 for the sampled time frames $t = 65$ s, 83 s and 99 s. At $t = 65$ s, the wave packet propagates from the wave generation zone, where a short wave is leading the wave train while the longer wave is chasing from behind. At $t = 83$ s, all the wave components superimpose into a focused wave with an amplified single peak with high velocities. At $t = 99$ s, the longer wave components surpass the shorter waves and the single peak decomposes into several components again. The entire process is clearly represented by the model.

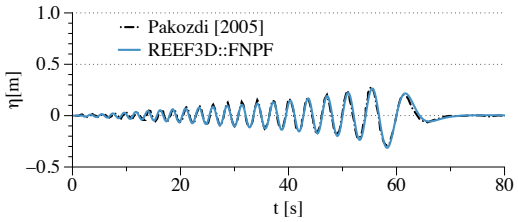

(a) wave gauge 1 at $x = 3.59$ m

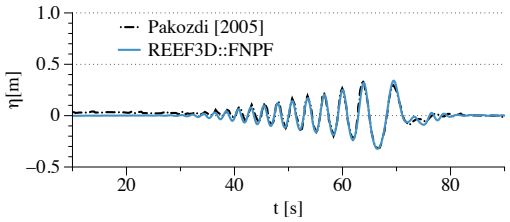

(b) wave gauge 2 at $x = 50.5$ m

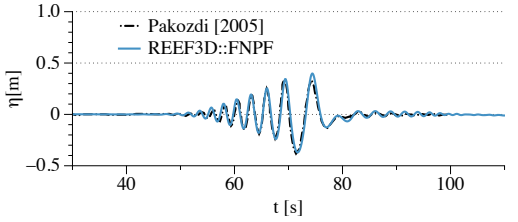

(c) wave gauge 3 at $x = 79.05$ m

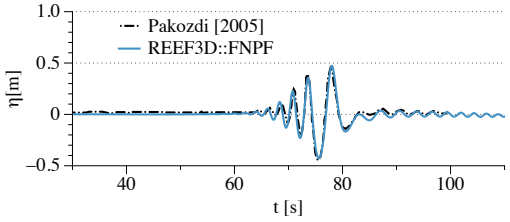

(d) wave gauge 4 at $x = 100.10$ m

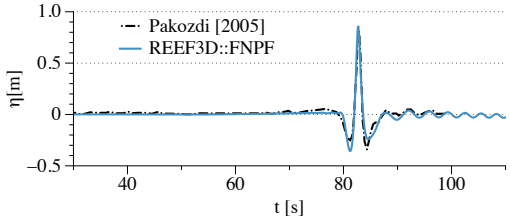

(e) wave gauge at the focus point at $x = 126.21$ m

Figure 8: The comparison between the simulated time series and the experimental measurements at all wave gauges in the numerical wave tank for the focusing wave packet.

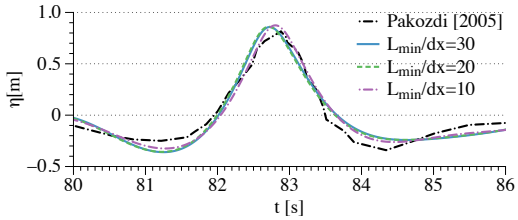

Figure 9: The grid convergence study at the focusing point for the wave packet propagation.

Three-hour irregular wave

The advantage of the potential flow solver is more prominent for long-duration simulations for obtaining statistical properties of a sea state. In order to gather statistical information on a wave field, it is necessary to perform a three-hour simulation at full scale. This is computationally demanding for Naiver-Stokes solvers. In this section, the proposed potential flow model is used to simulation a three-hour irregular sea state at intermediate water depth. The input spectrum is a JONSWAP spectrum with a peak enhancement factor of 3.0. The input wave has a significant wave height of $H_s = 4.5$ m, and peak period of $T_p = 12.0$ s. A constant water depth of 40 m is used. The two-dimensional wave tank is 1760 m long, corresponding to 8 wavelengths based on the peak period. The frequency range of $[0.75\omega_p, 2\omega_p]$ is used. The frequency limits represent the wave energy from 0.5% of the total energy to 99.5% of the total energy. Therefore, the chosen frequency range represents 99% of the total wave energy. The wave generation zone is located at the input boundary with the length of one wavelength corresponding to the lowest frequency. The numerical beach is located at the outlet boundary and has a length twice that of the wave generation zone. 30 vertical cells are used with vertical stretching in the σ-coordinate system. The horizontal resolution is 30 cells per wave length corresponding to the shortest wave with the highest frequency. The configuration results in a horizontal cell size of 2 m. The total number of cells is 26400. The simulation time is 12800 s, where the three-hour window from 2000 s to 12800 s is used for the data analysis. The wave elevation at the wave probe located five wave lengths (using the peak period) away is investigated for the chosen time window. The simulated spectrum is compared with the theoretical spectrum in Fig. 11. The horizontal velocity field of the simulation at $t = 12800$ s is shown in Fig. 12, where the surface elevation is amplified with

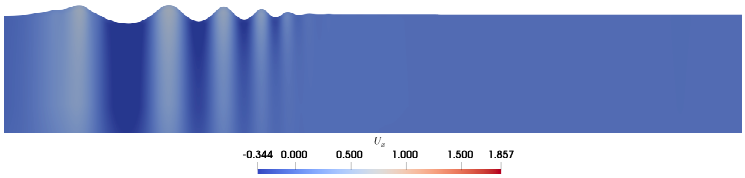

(a) Horizontal velocity at $t = 65$ s

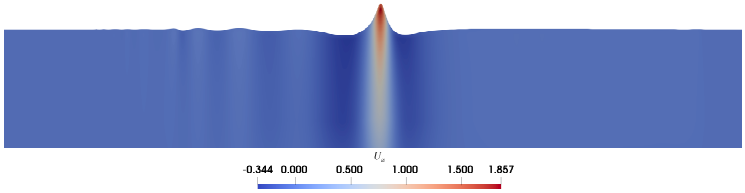

(b) Horizontal velocity at $t = 83$ s at the focusing time

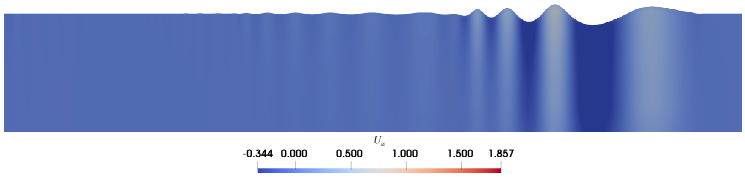

(c) Horizontal velocity at $t = 99$ s

Figure 10: The wave profile and the horizontal velocities (m/s) at different times during the evolution of the wave packet.

a factor of 10 for visualisation purpose. With 16 cores on supercomputer Vilje, the 12800 s simulation takes only 1.13 hour, which is three times faster than real time. The calculated significant wave height in the numerical wave tank is 4.456 m, the peak period is 11.95 s. With a compensation of 1% wave energy, the significant wave height becomes 4.50 m, exactly the same as the input value. The simulated irregular wave match the input H_s, T_p and the shape of the spectrum with high accuracy.

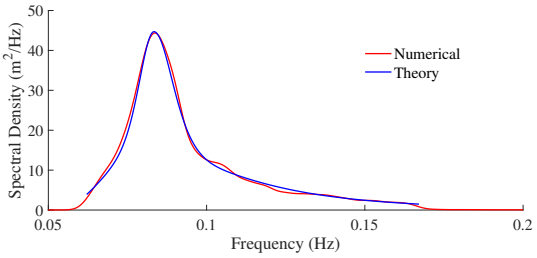

Figure 11: Simulated wave spectrum in comparison to the theoretical spectrum for the three-hour irregular wave simulation.

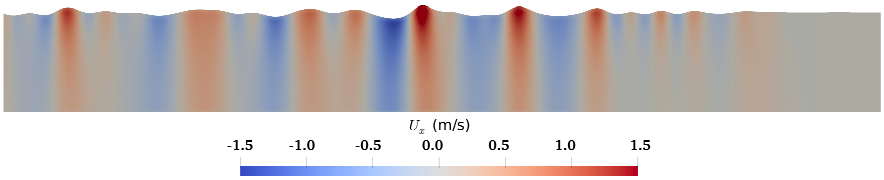

Figure 12: Horizontal velocities in the simulated irregular wave field in the entire numerical wave tank at $t = 12800$ s. Surface elevation is amplified with a factor of 10 for visualisation purpose.

4 Conclusions

The presented work introduces a new flexible fully-nonlinear potential flow solver REEF3D::FNPF in the numerical framework of the open-source hydrodynamics model REEF3D. The proposed model solves the Laplace equation together with the free surface boundary conditions and the bottom boundary condition using a finite difference method on a σ-coordinate system. The solution for the velocity potential is obtained with Hypres stabilized bi-conjugated gradient solver preconditioned with geometric multi-grid. High-order discretization schemes are used, such as a fifth-order WENO scheme in space and a third-order Runge-Kutta in time. The varying bottom is represented with the sigma coordinate grid. An efficient domain decomposition strategy is used for the parallel computation where the information between sub-domains is exchanged following an MPI protocol. The model is validated for the wave propagation over a submerged bar and the wave focusing from a wave packet. In both studies, the model provides favorable agreements with the experimental data. In addition, the model is able to perform simulations very fast with very limited computational resources, enabling complex simulations on personal computers or desktops. The model takes only one hour for the three-hour irregular wave simulation on 16 processors and obtained near identical statistical wave properties in comparison to the theoretical inputs. The model is proven to be accurate and computationally efficient for diverse and flexible scenarios with non-breaking waves. To further explore the model's potential, large-scale wave propagation over irregular natural topography and irregular coastline are to be investigated. A robust wave breaking algorithm is also to be introduced in the model for future studies.

Acknowledgements

The research work has been funded by the Norwegian Public Roads Administration through the E39 fjord crossing project (No. 304624).

References

Ahmad, N., Bihs, H., Myrhaug, D., Kamath, A. and ivind A. Arntsen (2018). Three-dimensional numerical modelling of wave-induced scour around piles in a side-by-side arrangement. *Coastal Engineering*, **138**, 132 – 151. ISSN 0378-3839. https://doi.org/10.1115/1.4045915https://doi.org/10.1016/j.coastaleng.2018.04.016.

Beji, S. and Battjes, J.A. (1993). Experimental investigation of wave propagation over a bar. *Coastal Engineering*, **19**, 151–162.

Bihs, H., Kamath, A., Alagan Chella, M. and Arntsen, Ø.A. (2019). Extreme Wave Generation, Breaking, and Impact Simulations Using Wave Packets in REEF3D. *Journal of Offshore Mechanics and Arctic Engineering*, **141**(4), 41802–41807. ISSN 0892-7219.

Bihs, H., Kamath, A., Chella, M.A., Aggarwal, A. and ivind A. Arntsen (2016). A new level set numerical wave tank with improved density interpolation for complex wave hydrodynamics. *Computers Fluids*, **140**, 191 – 208. ISSN 0045-7930.

Bingham, H.B. and Zhang, H. (2007). On the accuracy of finite-difference solutions for nonlinear water waves. *Journal of Engineering Mathematics*. ISSN 00220833. https://doi.org/10.1115/1.404591510.1007/s10665-006-9108-4.

Clauss, G.F. and Steinhagen, U. (1999). Numerical Simulation of Nonlinear Transient Waves and its Validation by Laboratory Data. In: *9th International Offshore and Polar Engineering Conference*.

Ducrozet, G., BONNEFOY, F., Le Touzé, D. and Ferrant, P. (2012). A modified High-Order Spectral method for wavemaker modeling in a numerical wave tank. *European Journal of Mechanics - B/Fluids*, **34**, http://dx.doi.org/10.1016/j.euromechflu.2012.01.017. https://doi.org/10.1115/1.404591510.1016/j.euromechflu.2012.01.017.

Ducrozet, G., Bonnefoy, F., Le Touzé, D. and Ferrant, P. (2016). HOS-ocean: Open-source solver for nonlinear waves in open ocean based on High-Order Spectral method. *Computer Physics Communications*, **203**, 245–254. https://doi.org/10.1115/1.404591510.1016/j.cpc.2016.02.017.

Ducrozet, G., Engsig-Karup, A.P., Bingham, H.B. and Ferrant, P. (2014). A non-linear wave decomposition model for efficient wavestructure interaction. part a: Formulation, validations and analysis. *Journal of Computational Physics*, **257**, 863 – 883. ISSN 0021-9991. https://doi.org/10.1115/1.4045915https://doi.org/10.1016/j.jcp.2013.09.017.

Engsig-Karup, A. and Bingham, H. (2009). Boundary-fitted solutions for 3d nonlinear water wave-structure interaction. In: *IWWWFB24*, 20.

Engsig-Karup, A., Bingham, H. and Lindberg, O. (2009). An efficient flexible-order model for 3D nonlinear water waves. *Journal of Computational Physics*, **228**, 2100–2118.

Engsig-Karup, A.P., Glimberg, S.L., Nielsen, A.S. and Lindberg, O. (2013). *Fast hydrodynamics on heterogenous many-core hardware*, 251294. Taylor Francis. ISBN 978-1-4665-7162-4. 2013;11.

Engsig-Karup, A.P., Madsen, M.G. and Glimberg, S.L. (2012). A massively parallel gpu-accelerated model for analysis of fully nonlinear free surface waves. *International Journal for Numerical Methods in Fluids*, **70**(1).

Glimberg, L.S., Engsig-Karup, A.P., Nielsen, A.S. and Dammann, B. (2013). Development of software components for heterogeneous many-core architectures. In: R. Couturier (Editor),

Designing Scientific Applications on GPUs, Lecture notes in computational science and engineering, 73–104. CRC Press / Taylor & Francis Group.

Grilli, S. (1996). Fully nonlinear potential flow models used for long wave runup prediction. *Long Wave Runup Models*.

Jacobsen, N.G., Fuhrman, D.R. and Fredsøe, J. (2012). A wave generation toolbox for the open-source CFD library: OpenFOAM. *International Journal for Numerical Methods in Fluids*, **70**(9), 1073–1088.

Janssen, C.F., Grilli, T. and Krafczyk, M. (2010). Modeling of Wave Breaking and Wave-Structure Interactions by Coupling of Fully Nonlinear Potential Flow and Lattice-Boltzmann Models. *Simulation*. ISSN 10986189. https://doi.org/10.1115/1.404591510.1016/j.jphotobiol.2011.03.017.

Jiang, G.S. and Shu, C.W. (1996). Efficient implementation of weighted ENO schemes. *Journal of Computational Physics*, **126**, 202–228.

Kamath, A., Bihs, H., Alagan Chella, M. and ivind A. Arntsen (2016). Upstream-cylinder and downstream-cylinder influence on the hydrodynamics of a four-cylinder group. *Journal of Waterway, Port, Coastal, and Ocean Engineering*, **142**(4), 04016002. https://doi.org/10.1115/1.404591510.1061/(ASCE)WW.1943-5460.0000339.

Li, B. and Fleming, C.A. (1997). A three dimensional multigrid model for fully nonlinear water waves. *Coastal Engineering*. ISSN 03783839. https://doi.org/10.1115/1.404591510.1016/S0378-3839(96)00046-4.

Madsen, P.A., Murray, R. and Sørensen, O.R. (1991). A new form of the Boussinesq equations with improved linear dispersion characteristics. *Coastal Engineering*, **15**, 371–388.

Mayer, S., Garapon, A. and Sørensen, L.S. (1998). A fractional step method for unsteady free surface flow with applications to non-linear wave dynamics. *International Journal for Numerical Methods in Fluids*, **28**, 293–315.

Mehmood, A., Graham, D.I., Langfeld, K. and Greaves, D.M. (2015). OpenFOAM Finite Volume Method Implementation of a Fully Nonlinear Potential Flow Model for Simulating Wave-Structure Interactions.

Mehmood, A., Graham, D.I., Langfeld, K. and Greaves, D.M. (2016). Numerical Simulation of Nonlinear Water Waves based on Fully Nonlinear Potential Flow Theory in OpenFOAM® -Extend.

Nwogu, O. (1993). Alternative form of Boussinesq equations for nearshore wave propagation. *Journal of Waterways, Port, Coastal, and Ocean Engineering*, **119**(6), 618–638.

Ong, M.C., Kamath, A., Bihs, H. and Afzal, M.S. (2017). Numerical simulation of free-surface waves past two semi-submerged horizontal circular cylinders in tandem. *Marine Structures*, **52**, 1 – 14. ISSN 0951-8339. https://doi.org/10.1115/1.4045915https://doi.org/10.1016/j.marstruc.2016.11.002.

Sasikumar, A., Kamath, A., Musch, O., Bihs, H. and Arntsen, Ø.A. (2018). Numerical Modeling of Berm Breakwater Optimization With Varying Berm Geometry Using REEF3D. *Journal of Offshore Mechanics and Arctic Engineering*, **141**(1), 011801. ISSN 0892-7219. https://doi.org/10.1115/1.404591510.1115/1.4040508.

Shu, C.W. and Osher, S. (1988). Efficient implementation of essentially non-oscillatory shock capturing schemes. *Journal of Computational Physics*, **77**, 439–471.

van der Vorst, H. (1992). BiCGStab: A fast and smoothly converging variant of Bi-CG for the solution of nonsymmetric linear systems. *SIAM Journal of Scientific Computing*, **13**, 631–644.

Wang, W., Kamath, A. and Bihs, H. (2018). CFD Simulations of Multi-Directional Irregular Wave Interaction With a Large Cylinder.